

# Spatial Transcriptomics of Meningeal Inflammation Reveals Variable Penetrance of Inflammatory Gene Signatures into Adjacent Brain Parenchyma


Reviewed Preprint

v2 • June 18, 2024

Revised by authors


Reviewed Preprint

v1 • July 11, 2023

Sachin P. Gadani, Saumitra Singh, Sophia Kim, Jingwen Hu, Matthew D. Smith, Peter A. Calabresi, Pavan Bhargava 

Division of Neuroimmunology, Department of Neurology, Johns Hopkins University School of Medicine, Baltimore, MD, USA • Solomon Snyder, Department of Neuroscience Johns Hopkins University School of Medicine, Baltimore, MD, USA

 [https://en.wikipedia.org/wiki/Open\\_access](https://en.wikipedia.org/wiki/Open_access)

 Copyright information

## Abstract

While modern high efficacy disease modifying therapies have revolutionized the treatment of relapsing-remitting multiple sclerosis, they are less effective at controlling progressive forms of the disease. Meningeal inflammation is a recognized risk factor for cortical grey matter pathology which can result in disabling symptoms such as cognitive impairment and depression, but the mechanisms linking meningeal inflammation and grey matter pathology remain unclear. Here, we performed MRI-guided spatial transcriptomics in a mouse model of autoimmune meningeal inflammation to characterize the transcriptional signature in areas of meningeal inflammation and the underlying brain parenchyma. We found broadly increased activity of inflammatory signaling pathways at sites of meningeal inflammation, but only a subset of these pathways active in the adjacent brain parenchyma. Sub-clustering of regions adjacent to meningeal inflammation revealed the subset of immune programs induced in brain parenchyma, notably complement signaling and antigen processing/presentation. Trajectory gene and gene set modeling analysis confirmed variable penetration of immune signatures originating from meningeal inflammation into the adjacent brain tissue. This work contributes a valuable data resource to the field, provides the first detailed spatial transcriptomic characterization in a model of meningeal inflammation, and highlights several candidate pathways in the pathogenesis of grey matter pathology.

### eLife assessment

Brain inflammation is a hallmark of multiple sclerosis. Using novel spatial transcriptomics methods, the authors provide **solid** evidence for a gradient of immune genes and inflammatory markers from the meninges toward the adjacent brain parenchyma in a mouse model. This **important** study advances our understanding of the mechanisms of brain damage in this autoimmune disease. However, the control mouse groups are not well designed to rule out confounding effects, a limitation that needs to be acknowledged and addressed.

<https://doi.org/10.7554/eLife.88414.2.sa2>

## Introduction

Multiple sclerosis (MS) is a chronic autoimmune disease of the central nervous system (CNS) characterized by a relapsing remitting and/or progressive course of demyelination, axonal injury, and neurologic dysfunction<sup>1</sup>. Highly efficacious disease modifying therapies have revolutionized the prevention and treatment of MS relapses, but are less effective at stopping hallmarks of MS progression such as brain atrophy<sup>2</sup>. Accumulating evidence points to a pivotal role for leptomeningeal inflammation (LMI) in contributing to this pathology<sup>3,4</sup>. LMI is found in all subtypes of MS, ranging histologically from disorganized collections of leukocytes to highly organized ectopic lymphoid follicles, and correlates with the presence of cortical grey matter demyelination, neurite loss, and decreased volume<sup>5</sup>. Grey matter pathology (GMP) has been linked to debilitating symptoms such as cognitive impairment and depression<sup>6</sup>, and tends to occur in spatial relation to areas of LMI. Indeed, the most common grey matter lesion location is directly sub-pial<sup>7</sup>, and there is a gradient of increased pathology towards the surface of the brain in MS patients<sup>8,9</sup>. Interestingly, GMP occurs without local blood-brain barrier disruption or robust infiltration of peripheral immune cells into the brain parenchyma<sup>10,11</sup>. LMI is therefore speculated to be a source of pro-inflammatory molecules that contribute to GMP<sup>12</sup>, but the pathway(s) involved remain unknown.

Several putative mechanisms linking LMI to GMP have been proposed. Magliozzi and colleagues identified increased expression of numerous cytokines and chemokines, including interferon gamma (IFN $\gamma$ ), tumor necrosis factor (TNF), interleukin (IL)-2, IL-22, CXCL13, and CXCL10, in the meninges and CSF of postmortem MS cases with high levels of meningeal inflammation and GM demyelination<sup>13</sup>. Microarray analysis of cortical lesions from MS cases with LMI revealed a shift in TNF signaling from TNFR1/TNFR2 and NF $\kappa$ B-mediated anti-apoptotic pathways towards TNFR1- and RIPK3-mediated pro-apoptotic/pro-necroptotic pathways<sup>14</sup>. In marmoset and rat models of experimental autoimmune encephalomyelitis (EAE), sub-pial cortical lesions were found with prominent microglial activation and immunoglobulin deposition on myelin sheaths<sup>15,16</sup>. Interestingly, complement deposition, one possible mechanism of immunoglobulin-related cellular injury, is not found in purely cortical grey matter lesions, in contrast to white or grey/white matter lesions<sup>17</sup>. Numerous other mediators of injury, including reactive oxygen and nitrogen species, metabolic stress, and excitotoxicity have been proposed to drive neurodegeneration in MS and may be at play in GMP.

Previous attempts to characterize the relation between LMI and GMP have been limited by the absence of spatially resolved data, which therefore lacks critical information about the anatomic relationship between LMI and the underlying brain parenchyma. Here, we present a spatial transcriptomic dataset and analysis in a mouse model of relapsing/remitting CNS autoimmunity

and meningeal inflammation, Swiss Jim Lambert (SJL) mouse EAE<sup>18</sup>. Our prior work in SJL EAE demonstrated meningeal areas of gadolinium contrast enhancement on magnetic resonance imaging (MRI) that correspond histologically to collections of B cells, T cells, and myeloid cells<sup>19</sup>. In the parenchyma adjacent to areas of meningeal inflammation we identified astrogliosis, activated microglia, demyelination and evidence of axonal stress and damage<sup>19</sup>. This work characterizes the spatially resolved transcriptome of LMI in the SJL EAE model system, revealing the subset of genes and gene sets active in the LMI that extend into the adjacent parenchyma and providing insights into immune pathways that could underlie sub-pial neurodegeneration.

## Materials and methods

### Animals

SJL/J mice were purchased from Jackson Laboratories for all experiments. All mice were maintained in a federally approved animal facility at Johns Hopkins University in accordance with the Institutional Animal Care and Use Committee. Female mice aged 7–8 weeks were used in all experiments and were housed in the animal facility for at least 1 week prior to the start of experiments.

### Induction of SJL EAE

Female SJL/J mice were immunized subcutaneously at two sites over the lateral abdomen with 100 µg PLP<sub>139-151</sub> peptide with complete Freund's adjuvant containing 4 µg/ml *Mycobacterium tuberculosis* H37RA (Difco Laboratories). Mice were weighed and scored serially to document disease course. Scoring was performed using the following scale: 0, normal; 1, limp tail; 2, hind limb weakness; 3, hind limb paralysis; 4, hind limb and forelimb weakness; and 5, death.

### MRI imaging

At weeks 6, 8, and 10 post immunization, a horizontal 11.7 T scanner (Bruker BioSpin) with a triple-axis gradient system (maximum gradient strength = 740 mT/m), 72 mm volume transmit coil and 4-channel receive-only phased array coil was used to image the mouse forebrain. During imaging, mice were anaesthetized with isoflurane together with mixed air and oxygen (3:1 ratio) and respiration was monitored via a pressure sensor and maintained at 60 breaths/min. Before imaging, 0.1 ml diluted Magnevist® (gadopentetate dimeglumine, Bayer HealthCare LLC, 1:10 with PBS) was injected. Scans were then analyzed to identify areas of meningeal contrast enhancement by two independent examiners (P.B., S.K.). We counted the number of areas of meningeal contrast enhancement on each individual MRI slice and used the cumulative number to represent the amount of meningeal contrast enhancement. All quantifications were performed by at least two independent examiners and their scores were averaged.

### Tissue preparation and spatial gene expression assay

At 11 weeks post-immunization, animals were euthanized in CO<sub>2</sub> chamber and perfused with cold PBS. Brains were dissected and one hemisphere drop fixed in isopentane cooled on dry ice. Fresh frozen brain samples were then cut coronally at a thickness of 10µm and placed on the capture area of Visium Gene Expression slides (v1; 10x Genomics). Each slide contained four 6.5 mm x 6.5 mm capture areas. Sample preparation was carried out according to manufacturer's instructions. After fixation with methanol at -20°C, Hematoxylin and Eosin (H&E) staining was performed for morphological analysis and spatial alignment of the sequencing data. After the enzymatic permeabilization, mRNA was captured by probes and cDNA generated. Barcoded cDNA was isolated using SPRIselect-cleanup (Beckman Coulter) and amplified. Amplified cDNA was fragmented and subjected to end-repair, poly-A-tailing, adaptor ligation, and 10x-specific sample indexing as per the manufacturer's instructions. Following assessment of RNA quality, sequencing

was performed using a Novaseq S2 100. Brains from four naïve and four EAE mice were used to prepare 5 and 6 individual slices per group, respectively, with once naïve mouse contributing two slices and two EAE mice contributing two slices.

## Spatial transcriptomics data processing

Each sample went through identical quality control processing steps. SpaceRanger software (v.1.3.1) was used to pre-process the sequencing data, aligning to the mm10-2020A reference transcriptome. Feature barcoded expression matrixes were used as input for downstream spatial transcriptomics analysis using Seurat (v.4.3.0) and SPATA2 (v.0.1.0)<sup>20</sup>. Data was loaded and analyzed using the Seurat, and all spots that were determined to not be over tissue were discarded using the filter.matrix option in Seurat's Load10XSpatial function. Spots with less than 250 measured genes and less than 500 unique molecular identifiers (UMIs) were filtered out. Data normalization and stabilization of sequence depth variance was performed on each sample using SCTransform with default parameters<sup>21</sup>. Sample data was then annotated and combined into a merged object for downstream quality control and analysis. Dimensionality reduction was performed using principal component analysis (PCA), followed by computation of shared nearest neighbors of the first 10 principal components and cluster identification (resolution 0.3). To visualize all spots in a two-dimensional plot, a UMAP was created with Seurat's RunUMAP function using the first 10 principal components. Cluster and sub-cluster enriched genes were identified with Wilcoxon tests as implemented in the FindMarkers function within Seurat. Differential gene expression between groups was attained using DESeq2 (v.1.38.2) on samples pseudobulked by biological replicate. Gene set enrichment analysis and visualization was performed using the gene ontology database<sup>22,23</sup> and the clusterProfiler package (v.4.6.0)<sup>24</sup>. Estimated signaling pathway activities were calculated for each spot with the top 500 genes of each pathway on SCTransformed data using the PROGENy package (v.1.20.0)<sup>25</sup>. For subclustering analysis, select clusters were subsetted before undergoing dimensionality reduction, neighbor calculation, cluster identification, marker identification, and gene set enrichment as described above. Trajectory gene and gene set modeling analysis was performed with the SPATA2 package. Spatial trajectories were drawn in EAE slices from the center of cluster 11 to the centromedial nucleus of thalamus. Gene and gene-sets were analyzed along these trajectories using the assessTrajectoryTrends function within SPATA2.

## RNAscope

Brain tissue was collected from N = 3 naïve or EAE (11 weeks post immunization) SJL mice after transcardial perfusion with 4% PFA. Brains were post-fixed for 48 hours and then dehydrated via sucrose gradient over 48 hours before freezing in OCT. Fourteen µm thick tissue sections were collected directly onto Superfrost+ slides (Fisherbrand, Cat. No. 22-037-246). The RNAscope assay was then carried out using the Multiplex Fluorescent Reagent Kit v2 (Advanced Cell Diagnostics, Cat. No. 323100) per the manufacturer's instructions. Briefly, tissue sections underwent dehydration in an ethanol gradient, peroxide blocking, and antigen retrieval steps. Antigen retrieval was performed using a steamer at 100°C and the epitope retrieval solution provided by the manufacturer. The mRNA in the tissue was hybridized to RNAscope probes (Advanced Cell Diagnostics) against: *C3* (Cat. No. 417841-C3), *Fcgr3* (Cat. No. 587241), *B2m* (Cat. No. 415191-C2), *Cd74* (Cat. No. 437501-C3), and *Gfap* (Cat. No. 313211) for 2 h at 40°C and stored overnight in 5x saline sodium citrate. Next, amplification steps were performed according to the manufacturer's instructions. Fluorescent labeling was performed with TSA Vivid Fluorophore 520, TSA Vivid Fluorophore 570, and TSA Vivid Fluorophore 650 (all at 1:2000 dilution). Slides were washed and mounted with ProLong Gold Antifade Mountant (ThermoFisher, Cat. No. P36830). Slides were imaged via confocal microscopy (Zeiss LSM900). Positive cells were manually labeled in ImageJ (NIH). The x-y coordinate of each cell was used to determine the shortest distance to areas of leptomeningeal inflammation in R. Distances were batched at intervals of 50µm. Non-linear regression of the batched data was computed using the stats::nls function and the formula  $percentage \sim a * distance ^ b$ .

## RNAseq statistics and data visualization

Plots were generated and statistics calculated using R (v.4.2.2) and Rstudio (v.2022.07.2). Bar plots, box plots, MA plots, Venn diagram, and dot plots were produced with ggplot2 (v.3.4.0); heat maps were produced with pHeatmap (v.1.0.12) and enrichplot (v.1.18.4)<sup>26</sup>; spatial feature plots and dimensionality reduction plots were produced with Seurat; tree plots were produced with enrichplot, and trajectory heatmaps were produced with SPATA2.

All reported P-values adjusted for multiple comparisons were corrected using the Benjamini-Hochberg method<sup>27</sup> unless otherwise specified. The number of samples in the EAE and naïve groups was chosen based on expected levels of variability in prior experiments.

## Results

We tracked the development of LMI during SJL EAE using contrast enhanced serial MRI imaging. MRI data was then used to target areas of LMI for spatial transcriptomics (**Figure 1A**). Mice developed a characteristic relapsing pattern of neurologic impairment, and contrast-enhanced MRI was performed at weeks 6, 8, and 10 post immunization (**Figure 1B-C**). In the SJL EAE model, contrast enhancing meningeal lesions are most frequently found in the intrapeduncular cistern, quadrigeminal cistern, and the cleft between the hippocampus and medial geniculate nucleus<sup>19,28</sup> (**Figure 1D**). Lesion number remained stable throughout the disease course independent of EAE score (Supplemental Figures 1A-B).

Brain slices were collected from four naïve mice and four EAE mice 11 weeks postimmunization and used to prepare five and six samples for spatial transcriptomics, respectively. H&E staining confirmed the presence of meningeal inflammation in the areas of contrast enhancement, as we had previously observed<sup>19</sup> (**Figure 1E**). Data from all samples were of high quality and read depth when assessed by treatment group (Supplemental Figure 2A-C) or sample (Supplemental Figure 2D-E). There was expected anatomic variability in number of read counts and number of features per spot, with relatively low counts and features in white matter as compared to the cortex or hippocampus (Supplemental Figure 2F-G), and spots had similar degrees of average complexity between EAE and naïve samples (Supplemental Figure 2H). UMAP clustering revealed no significant independent effect of sample (Supplemental Figure 2I) or slide (Supplemental Figure 2J). Numerous genes were differentially expressed between EAE and naïve slices as estimated by DESeq2 on samples pseudobulked by biological replicate (Supplementary Table 1; Supplemental Figure 2K), including genes associated with the complement cascade, immune infiltration, antigen presentation, and astrocyte activation (**Figure 1F**).

We next explored the activity of a broad range of pathways using the pathway responsive genes (PROGENy) method<sup>25</sup> (**Figure 2A**). Inflammatory pathways related to TNF, JAK-STAT, and NFκB signaling were upregulated in EAE compared to naïve, with peak activity around sites of meningeal inflammation (**Figure 2B-C**). Pathways related to Trail and PI3K were downregulated in EAE compared to naïve (**Figure 2D-E**), and TGFβ pathway activity was unchanged between groups (**Figure 2D-E**).

To focus our analyses on foci of meningeal inflammation specifically, we performed unbiased UMAP clustering on the spatial transcriptomic dataset and identified 12 distinct clusters (**Figure 3A**). Grouping the dimensional reduction UMAP plot by EAE and naïve revealed that cluster eleven (C11) was restricted to EAE samples (**Figure 3B**). C11 makes up 1–5% of the total spots in those samples (**Figure 3C**), or about 20–120 total spots, and was significantly enriched in EAE relative to naïve samples (**Figure 3D**). Visualizing the clusters using spatial feature plots confirmed that most clusters map consistently to specific anatomic regions and were similar



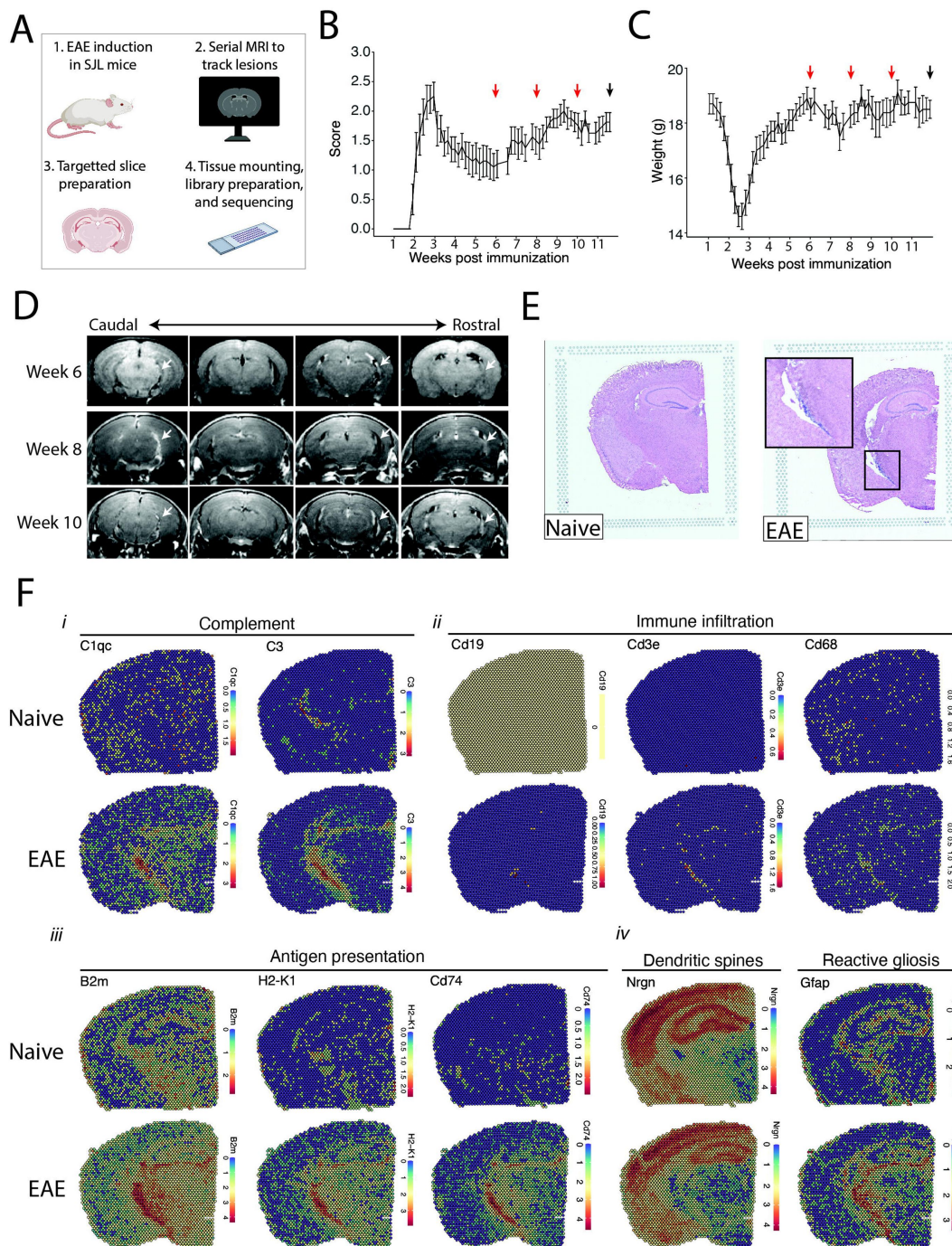


**Figure 1**

### MRI guided spatial transcriptomics of meningeal-based inflammation in SJL EAE.

(A) Schematic describing the experimental paradigm. SJL mice underwent brain MRI 6-, 8-, and 10 weeks post immunization with PLP<sub>139-151</sub>. Brain slices from regions with meningeal inflammation were collected and processed for spatial transcriptomics on the 10x Genomics platform. (B–C) Behavior scores (B) and mouse weights (C) of the EAE cohort. Red arrows indicate MRI time points, black arrow indicates time of tissue harvesting (N = 4). (D) Representative post-contrast MRI brain images, white arrows indicate areas of meningeal-based inflammation. (E) Representative images of H&E-stained tissue sections mounted on spatial transcriptomics slides (left, naïve; right, EAE). (F) Spatial feature plots from naïve (top row) and EAE (bottom row) representative samples demonstrate altered expression of genes related to complement (i), immune infiltration (ii), antigen presentation (iii), dendritic spines, and astrocyte activation (iv).

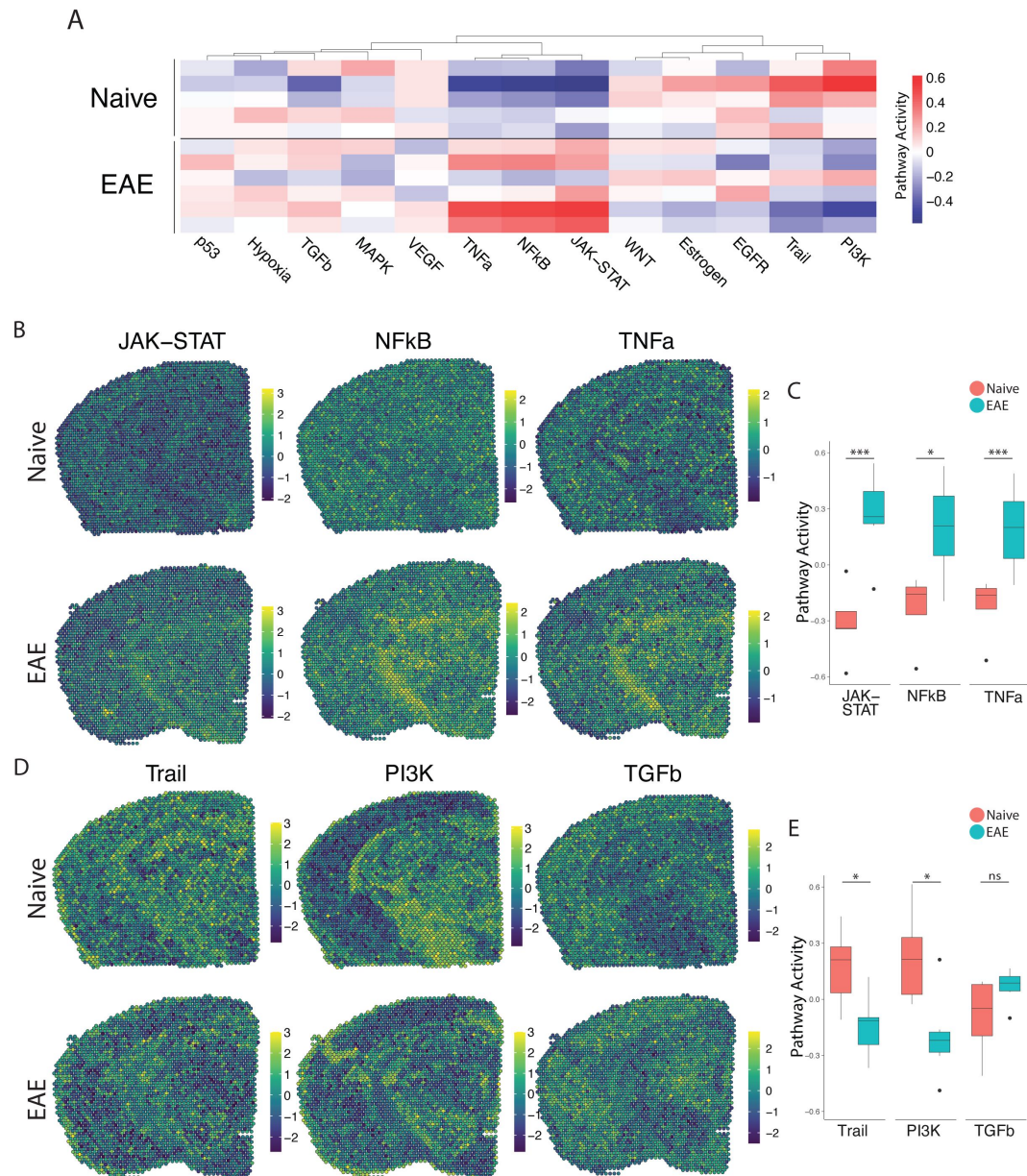


**Figure 2**

**PROGENy analysis reveals spatially restricted pathway activity differences between naïve and EAE.**

(A–B) Heat map displaying averaged PROGENy pathway analysis results. (C) Representative spatial plot showing activity of the JAK-STAT, NFkB, and TNFa signaling pathways. (D) Comparison of JAK-STAT, NFkB, and TNFa pathway activities between groups. (E) Representative spatial plot showing activity of the Trail, PI3K, and TGFb signaling pathways. (F) Comparison of Trail, PI3K, and TGFb pathway activities between groups. (Naïve mouse N = 4, sample N = 5; EAE mouse N = 4, sample N = 6; multiple T tests corrected for multiple comparisons with the Benjamini, Krieger, and Yekutieli method; \* p < 0.05, \*\* p < 0.01, \*\*\* p < 0.001).



between naïve and EAE (**Figure 3E** [↗](#); Supplementary Figure 3A). C11 overlapped with previously noted areas of meningeal MRI enhancement, suggesting that C11 represents areas of meningeal inflammation (**Figure 3E** [↗](#); Supplementary Figure 3B-D). We compared the gene expression in C11 to other clusters and found 132 upregulated genes and 70 downregulated genes ( $p < 0.05$ ; Log2 fold change  $> 1$ ; **Figure 3F** [↗](#)). Inflammation-related genes were prominently represented in C11 relative to other clusters (Supplementary Table 2), with top genes including *Cd74*, *C3*, and *Gfap* (**Figure 3G** [↗](#); Supplementary Figure 3E). The presence of glial genes such as *Gfap* within cluster 11 likely represents areas of subpial brain parenchyma included within the cluster. Immunoglobulin genes, which are highly expressed in areas of human grey matter pathology,<sup>14</sup> [↗](#) were also upregulated in C11 (Supplementary Figure 3F). We next performed gene set enrichment analysis of C11 spots using the Gene Ontology (GO) database<sup>22</sup> [↗](#),<sup>23</sup> [↗](#), finding 538 variable gene sets (adjusted P-value  $< 0.05$ ; Supplementary Table 3). Among the most prominently enriched gene sets were those involved in antigen processing and presentation, complement activation, lymphocyte activation, and cytokine production and response (**Figure 3H** [↗](#)).

After establishing the defining transcriptomic features of meningeal inflammation in our model, we next sought to characterize inflammatory changes in the adjacent CNS parenchyma. We performed unbiased sub-clustering of each cluster in turn and found EAE-specific subclusters and differentially expressed genes within clusters 1 and 2. These subclusters were labelled 1\_3, 1\_4, and 2\_6 (**Figure 4A-B** [↗](#); Supplemental Figure 4) and represent regions of the thalamus and hypothalamus (**Figure 4C** [↗](#)).

Next, we assessed whether EAE-specific subclusters were physically closer to meningeal inflammation than other related subclusters. The distance between the average location in each subcluster to the nearest point of C11 was calculated. In the subclusters of cluster 1, we found no difference in proximity to C11 between EAE-specific subclusters vs. subclusters present in EAE and naïve. However, in subclusters of cluster 2, the EAE-specific subcluster was significantly closer to C11 on average compared to other subclusters (**Figure 4D** [↗](#)). To explore which pathways were activated in these subclusters, we performed gene set enrichment analysis using the GO database (**Figure 4E-G** [↗](#); Supplementary Tables 4-6). All subclusters displayed enrichment of GO genesets related to inflammation, antigen processing and presentation, and humoral immunity. Interestingly, pathways related to neuron death, cellular stress, and negative regulation of cellular processes were also enriched (**Figure 4E-G** [↗](#); Supplementary Figure 5). Interestingly, other pathways related to cell death, including positive regulation of apoptotic process or programmed cell death, were upregulated in subcluster 1\_3 but downregulated in subcluster 1\_4, suggesting spatially variable survival signals (Supplementary Tables 4-5). Overall, 31 upregulated pathways were conserved between cluster 11 and subclusters 1\_3, 1\_4, 2\_6 (**Figure 4H** [↗](#)). We found prominent conserved upregulation of pathways related to adaptive/B-cell mediated immunity, antigen processing and presentation, cell killing, and others (**Figure 4I** [↗](#)).

Our pathway analysis of meningeal inflammation and areas of inflamed adjacent brain parenchyma suggested that inflammatory signals increased in meningeal inflammation could have variable ‘penetration’ into the adjacent brain. We sought to test this using spatial trajectory gene/gene set expression modelling available within the SPATA2 software package<sup>20</sup> [↗](#). Trajectories were drawn in EAE samples from the largest region of meningeal inflammation to the central thalamus (**Figure 5A** [↗](#)). Gene and gene set expression levels were then evaluated along the length of these trajectories and compared to ideal patterns of expression, as demonstrated for representative genes *B2m* and *C3* (**Figure 5B-E** [↗](#)). The difference between gene or gene set expression and the ideal patterns, here “logarithmic descending” or “gradient descending”, is represented by the residual line (**Figures 5B** [↗](#), **5E**). The area under the residual curve (residual AUC) is therefore inversely proportional to fit for the given gene or gene set and ideal pattern. *C3* expression declines rapidly along the trajectory and the logarithmic descending residual AUC is lower than gradient descending residual AUC (**Figure 5E** [↗](#)), while *B2m* follows a less steep decline and fits the two patterns similarly (**Figure 5C** [↗](#)). Trajectory analysis of gene sets enriched in



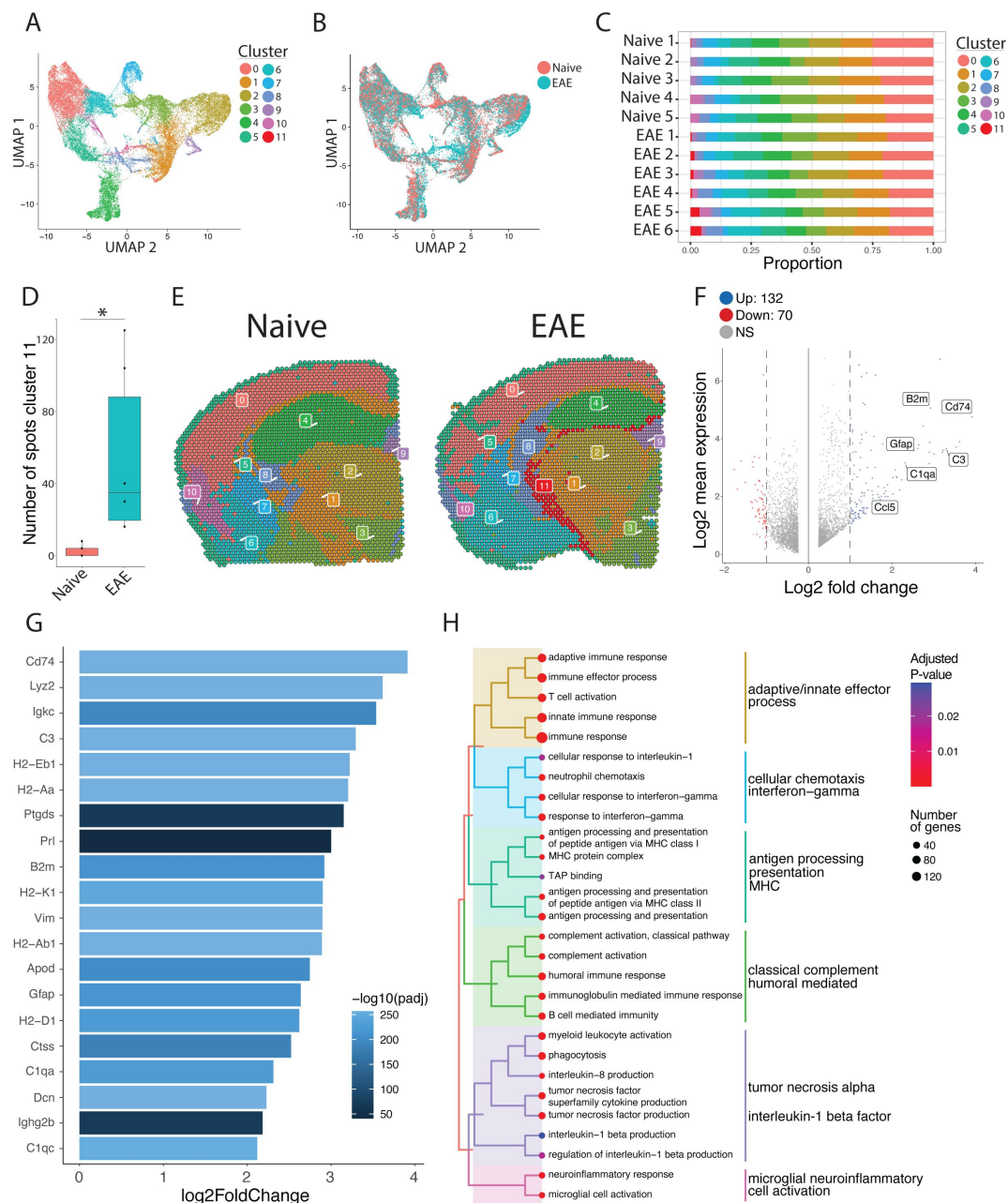


**Figure 3**

### Unbiased clustering reveals a group of spots enriched in inflammatory genes.

(A–B) UMAP dimensionality reduction plots colored by (A) cluster or (B) group. (C) Bar plot showing the proportion of spots in each cluster by sample. (D) Number of spots in cluster 11 by group (N = 11; Student’s two-tailed T test). (E) Representative spatial feature plots of naïve and EAE samples showing the spatial distribution of each cluster. (F) MA plot comparing differences in gene expression between cluster 11 and all other clusters averaged across samples. Red and blue spots represent genes in cluster 11 that are significantly increased or decreased, respectively (adjusted p-value < 0.05, log 2 fold change > 1). (G) Bar plot of top 15 genes enriched in cluster 11 compared to other clusters. (H) Tree plot displaying gene set enrichment results using the gene ontology (GO) database. Spots in cluster 11 were compared to other spots and gene set sizes ranging from 10–500 were included (adjusted p-value < 0.05).

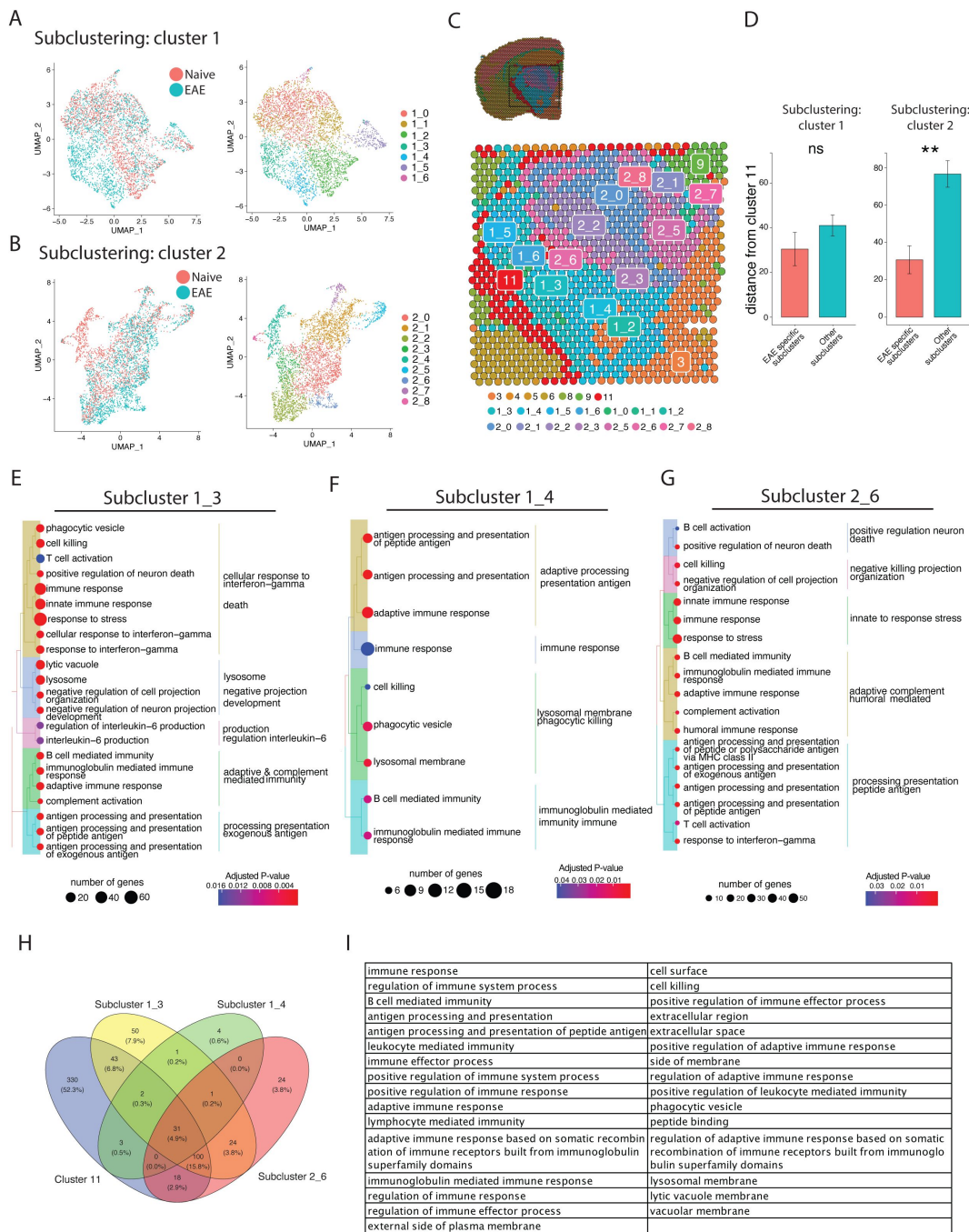


**Figure 4**

### Subclustering of spots adjacent to meningeal immune follicles reveals a subset of active immune patterns.

(A) UMAP dimensionality reduction plots showing subclustering of cluster 1 colored by (left) group or (right) cluster. (B) UMAP dimensionality reduction plots showing subclustering of cluster 2 colored by (left) group or (right) cluster. (C) Representative spatial feature plot showing the locations of cluster 1 and 2 subclusters. (D) Distance from the center of indicated subclusters to the nearest point of cluster 11 (N = 11; Student's two-tailed T-Test). (E– G) Tree plot displaying gene set enrichment results using the gene ontology (GO) database for subcluster 1\_3 (E), 1\_4 (F), and 2\_6 (G) compared to other spots in their respective clusters. (H) Venn diagram shows overlap of significantly enriched GO gene sets between cluster 11 and subclusters 1\_3, 1\_4, and 2\_6, with (I) 31 gene sets elevated in all. GO gene set of size ranging from 10–500 were included (adjusted p-value < 0.05).

meningeal inflammation and adjacent brain parenchyma was performed in this way, and the average residual AUC was calculated for gradient descending/ascending and logarithmic descending/ascending patterns (**Figure 5Fi** [↗](#)). As expected, all gene sets fit descending patterns better than ascending ones. There was variability in fit to the gradient descending pattern of expression, representing a more gradual decline in pathway enrichment along the trajectory, with gene sets related to antigen processing and presentation, cell killing, interleukin 6 production, and interferon gamma response having the best fit (**Figure 5Fi** [↗](#)). Enrichment score trajectory heatmap of a representative sample corroborates this, showing increased activity farther along the spatial trajectory for these gene sets (**Figure 5Fii** [↗](#)).

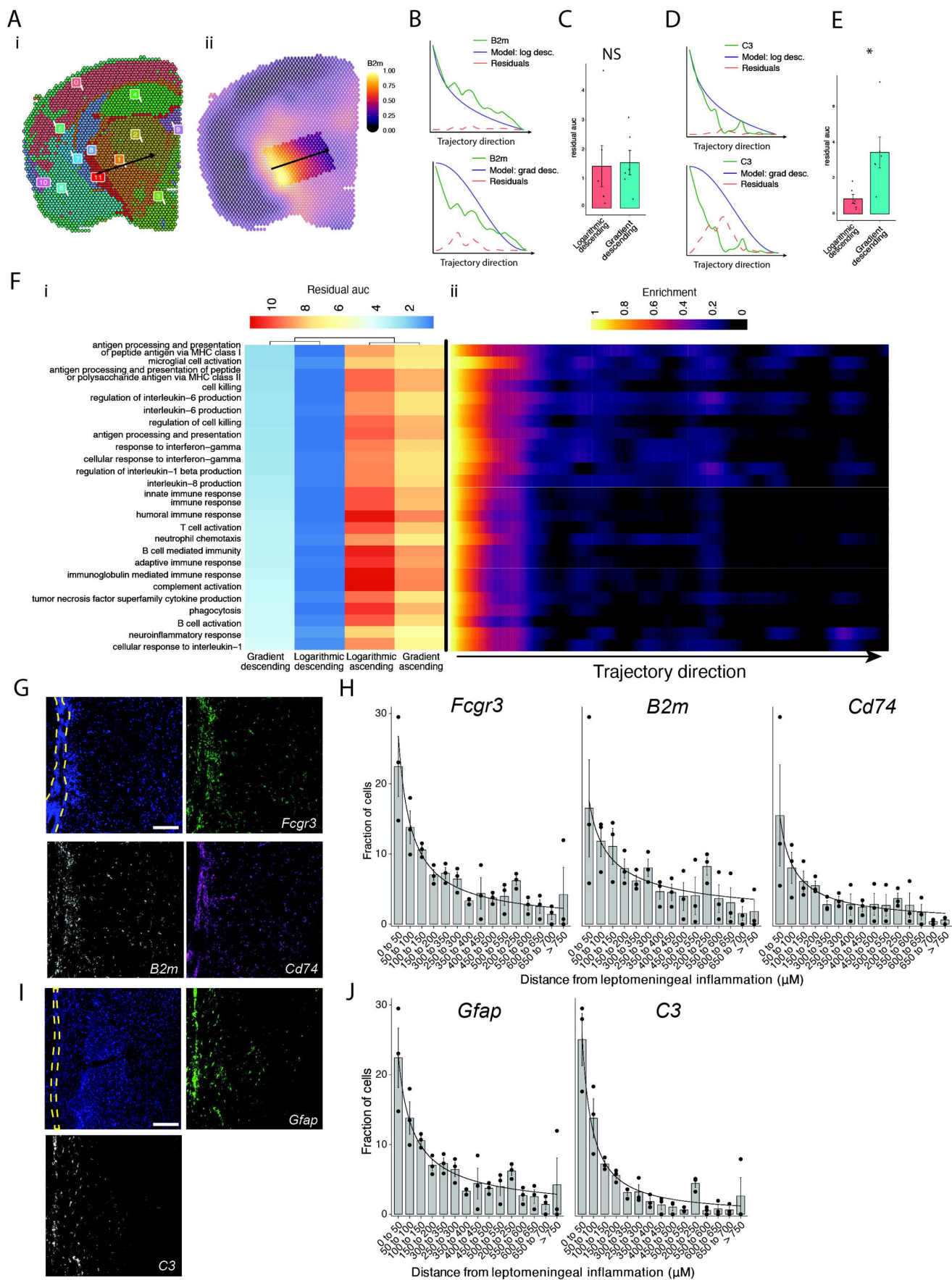




Figure 5

### Trajectory analysis reveals gradients of gene expression originating from meningeal lymphoid follicles.

(A) Trajectories were drawn based on spatial cluster plot (i) from C11 to C2 (ii). (B) Representative plot of *B2m* relative expression along the trajectory length. Green line: *B2m* expression; black line: ideal model fit, “logarithmic descending” (top) or “gradient descending” (bottom); red line: residual area under the curve (AUC) representing the difference between *B2m* expression and the ideal model. (C) Barplot showing residual AUC of *B2m* relative expression along the trajectory direction compared to “logarithmic descending” or “gradient descending” (Student’s two-tailed T-test). (D) Representative plot of *C3* relative expression along the trajectory length. Green line: *C3* expression; black line: ideal model fit, “logarithmic descending” (top) or “gradient descending” (bottom); red line: residual area under the curve (auc) representing the difference between *C3* expression and the ideal model. (E) Barplot showing residual AUC of *C3* relative expression along the trajectory direction compared to “logarithmic descending” or “gradient descending” (Student’s T-test). (F) Genesets that were previously identified as significantly enriched in C11 were selected for trajectory analysis. Residual AUCs were calculated for “logarithmic descending”, “gradient descending”, “logarithmic ascending”, and “gradient ascending” ideal fits and displayed on (i) a heatmap sorted by “gradient descending”. (ii) Representative feature plot demonstrating deeper penetration of upper genesets (related to antigen presentation and processing, microglial activation, IL-6 production, interferon gamma) response relative to other gene sets (B cell activation, T cell activation, TNF production, complement, humoral immune response). (G, I) Representative images of RNAscope labeling for (G) *Fcgr3*, *B2m*, *Cd74*, and (I) *Gfap*, *C3* in SJL mice 11 weeks after EAE induction. Yellow dashed lines indicate the areas of leptomeningeal inflammation, scale bars represent 100μM. (H, J) Barplots representing the percent of marker-positive cells present at distances from leptomeningeal inflammation. Lines represent best fit curves from exponential regression. N = 3 animals per group; bars represent mean, error bars represent standard error.

We next validated this variability in pattern of expression in a separate cohort of SJL mice with EAE using RNAscope to label selected transcripts related to glial activation (*Fcgr3* and *Gfap*) antigen presentation (*B2m* and *Cd74*) and complement (*C3*) (Figure 5G–I). Consistent with our spatial transcriptomics data, each of these transcripts was substantially induced in EAE as compared to Naïve (Supplemental Figure 6). We quantified the shortest distance of each targetpositive cell from the region of LMI (Figure 5H–J). For all transcripts, the number of positive cells decreased with distance exponentially. Exponential regression was applied to find the best fit curves of the data, modeled by the equation  $y = a * x^b$  where  $y$  is percentage of cells,  $x$  is distance from LMI. The exponential constant  $b$  reflects the rate of decrement and had higher absolute value in *C3* ( $b = -1.13$ ) relative to *B2m* ( $b = -0.59$ ) (Table 7).

## Discussion

Meninges-restricted inflammation in MS is intimately related to subpial grey matter demyelination<sup>3</sup>, atrophy, and neurocognitive symptoms, but therapeutically targeting this aspect of the disease is challenging due to poorly understood pathologic mechanisms. Here, we present spatial transcriptomics analysis in a mouse model of LMI, finding a broad swath of inflammatory pathways upregulated at foci of LMI and a subset of them upregulated in the nearby brain parenchyma. Notably, genes related to B cell mediated responses and antigen processing and presentation were upregulated in inflammatory parenchymal subclusters. Variable penetrance of inflammatory pathway activity was evident when analyzing the expression pattern of genesets along a linear trajectory from LMI into the CNS parenchyma, where antigen processing and presentation, interleukin 6 production, and the IFNγ response pathway activity followed a more gradual decline as compared to other pathways.

An important limitation of the spatial transcriptomics method used in this study is the spatial resolution of each spot. Since each spot is ~55µm in diameter it is likely that multiple cells are captured in each one. The simultaneous addition of single cell analysis would facilitate deconvolution of cell types within each spot. Furthermore, some spots of the borders of anatomic structures are likely to include both regions. This is exemplified by the spots within cluster 11, which in this study mainly represent meningeal inflammation, also being enriched in glial genes such as *Gfap*. Other methods of spatial RNA analysis exist that allow single cell resolution, but to date are probe-based and therefore limited by the number of genes assessed.

Prior work supports roles for pathways identified in our dataset, including B cell and IFNγ mediated responses, in contributing to neurodegeneration in MS. LMI in MS is rich in B cells, and the critical role of B cells in MS has been underscored by the success of B cell depletion in relapsing and progressive MS. Recent studies have proposed numerous mechanisms whereby B cells could contribute to cortical pathology, including indirectly through activation and inflammatory polarization of T cells, myeloid cells, and astrocytes or directly through production of neurotoxic cytokines or antibodies<sup>29</sup>. B cell culture supernatants from MS patients, but not healthy controls, are toxic to rat and human neurons and oligodendrocytes with this effect being mediated by the extracellular vesicle (EV) fraction of the supernatants<sup>30,31</sup>. B cells are also sources for inflammatory cytokines, such as IL-6 and GM-CSF, and antibodies, which are speculated to contribute to GMP<sup>29</sup>.

The role of IFNγ in the pathogenesis of MS and EAE is complex, and likely has stage specific protective and pathologic effects<sup>32</sup>. Its prominent upregulation in EAE was initially considered evidence of its pathogenic nature, but subsequent experiments showed that it was pathogenic during the initiation phase but protective later in the course<sup>32</sup>. IFNγ signaling and subsequent upregulation of antigen processing and presentation on glia has been identified as a mechanism that could lead to remyelination failure and subsequent neuronal loss<sup>33</sup>. Oligodendrocyte precursor cells (OPCs) upregulate antigen presentation and cross-presentation pathways in response to IFNγ, promoting inflammation and making them susceptible to CD8+ T cell killing<sup>33</sup>. Upregulation of genes for self-antigen presentation has also been noted in neurons and oligodendrocyte lineage (OL) cells in post-mortem MS single nucleus RNAseq<sup>34</sup>, and OL cells in EAE<sup>35–38</sup>. Recent work also assessed subcortical white matter lesions from postmortem MS cases via spatial transcriptomics, finding prominent elevation of TNF signaling, in agreement with presented results in the SJL EAE model<sup>39</sup>.

While SJL EAE models many features of LMI in MS<sup>18</sup>, there are important differences that limit the direct translation of these results to MS. The majority of LMI identified in mice with SJL EAE in our experiments occurred in subarachnoid cisterns, and as a result prominently affected areas of deep grey matter including thalamus and hypothalamus as opposed to cortical lesions also seen in MS. Notably, neuronal loss in the thalamus and other deep grey nuclei does occur in MS with a similar ‘surface-in’ gradient of neuronal injury, thought to also be related to toxic CSF-derived factors<sup>40,41</sup>. Demyelination, microglia and astrocyte activation, and neuronal loss are evident in the parenchyma adjacent to LMI in SJL EAE<sup>19,42</sup>. We also noted some variability in the extent and location of LMI, which is unavoidable in EAE. While other animal models of LMI, such as directly injecting inflammatory cytokines into the meninges/cortex, produce more predictable regions of LMI, they involve traumatic injury to the brain and typically lack folliclelike structures<sup>43</sup>. Notably, novel rodent models of cytokine-mediated LMI have recently been developed, including virus-mediated meningeal overexpression of TNF and IFNγ or subarachnoid injection of recombinant Lymphotoxin-α, were recently developed and exhibit lymphoid like structures<sup>44,45</sup>. Spatially resolved analyses of these models could provide additional insights into sub-pial pathology during neuroinflammation.

This work is the first to characterize a mouse model of LMI and grey matter injury using spatial transcriptomics, and in addition to the analysis presented here contributes a publicly available dataset for future research. We highlight the importance of antigen processing and presentation and complement signaling, which are prominently upregulated in sub-pial grey matter, in our model. Future studies should focus on spatial transcriptomics in post-mortem or biopsied human tissue. While access to appropriate samples remains a significant barrier, recent advances in RNA extraction from formalin fixed paraffin embedded tissues<sup>46,47</sup> will allow for the use of large banks of historically collected and preserved samples and could dramatically improve availability.

## Acknowledgements

We thank members of the Calabresi lab for their valuable comments during multiple discussions of this work. We thank the Johns Hopkins Medicine Single Cell and Transcriptomics Core for their assistance with planning and data acquisition. We thank the Dong lab at Johns Hopkins School of Medicine, Snyder Department of Neuroscience, for assistance with RNAscope experiments. We acknowledge the contribution of animals used in this research study.

## Ethics approval and consent to participate

All animal studies followed national and institutional guidelines for human animal treatment in compliance with the Johns Hopkins ACUC.

## Availability of data and material

Data availability: spatial transcriptomic data presented in this study is available on the Gene Expression Omnibus data (series record GSE236963).

## Competing interests

The authors have no competing interests to disclose.

## Funding

This work was supported in part by an investigator-initiated grant from EMD-Serono to PB, a Harry Weaver Neuroscience Scholar award to PB and a fellowship grant from the National Multiple Sclerosis Society and the American Brain Foundation (FAN-2106-37832) to SPG.

## Authors' contributions

SPG, SS, SK, MS, PAC, and PB conceived and designed the experiments. SS, SK, JH, and MS performed the experiments and collected the data. SPG and MS analyzed the data. SPG, SS, PAC, and PB wrote the manuscript. All authors reviewed and suggested improvements to the manuscript.

## References

1. Reich D. S., Lucchinetti C. F., Calabresi P. A. (2018) **Multiple Sclerosis** *New England Journal of Medicine* **378**:169–180
2. Faissner S., Plemel J. R., Gold R., Yong V. W. (2019) **Progressive multiple sclerosis: from pathophysiology to therapeutic strategies** *Nat Rev Drug Discov* **18**:905–922
3. Howell O. W., et al. (2011) **Meningeal inflammation is widespread and linked to cortical pathology in multiple sclerosis** *Brain* **134**:2755–2771
4. Absinta M., et al. (2015) **Gadolinium-based MRI characterization of leptomeningeal inflammation in multiple sclerosis** *Neurology* **85**:18–28
5. Wicken C., Nguyen J., Karna R., Bhargava P. (2018) **Leptomeningeal inflammation in multiple sclerosis: Insights from animal and human studies** *Multiple Sclerosis and Related Disorders* **26**:173–182
6. Geurts J. J., Barkhof F. (2008) **Grey matter pathology in multiple sclerosis** *The Lancet Neurology* **7**:841–851
7. Bø L., Vedeler C. A., Nyland H. I., Trapp B. D., Mørk S. J. (2003) **Subpial Demyelination in the Cerebral Cortex of Multiple Sclerosis Patients** *J Neuropathol Exp Neurol* **62**:723–732
8. Magliozzi R., et al. (2010) **A Gradient of neuronal loss and meningeal inflammation in multiple sclerosis** *Ann Neurol* **68**:477–493
9. Mainero C., et al. (2015) **A gradient in cortical pathology in multiple sclerosis by in vivo quantitative 7 T imaging** *Brain* **138**:932–945
10. van Horssen J., Brink B. P., de Vries H. E., van der Valk P., Bø L. (2007) **The Blood-Brain Barrier in Cortical Multiple Sclerosis Lesions** *J Neuropathol Exp Neurol* **66**:321–328
11. Bø L., Vedeler C. A., Nyland H., Trapp B. D., Mørk S. J. (2003) **Intracortical multiple sclerosis lesions are not associated with increased lymphocyte infiltration** *Mult Scler* **9**:323–331
12. Pikor N. B., Prat A., Bar-Or A., Gommerman J. L. (2016) **Meningeal Tertiary Lymphoid Tissues and Multiple Sclerosis: A Gathering Place for Diverse Types of Immune Cells during CNS Autoimmunity** *Front Immunol* **6**
13. Magliozzi R., et al. (2018) **Inflammatory intrathecal profiles and cortical damage in multiple sclerosis: Intrathecal Inflammation in MS** *Ann Neurol* **83**:739–755
14. Magliozzi R., et al. (2019) **Meningeal inflammation changes the balance of TNF signalling in cortical grey matter in multiple sclerosis** *Journal of Neuroinflammation* **16**
15. Storch M. K., et al. (2006) **Cortical demyelination can be modeled in specific rat models of autoimmune encephalomyelitis and is major histocompatibility complex (MHC) haplotype-related** *J Neuropathol Exp Neurol* **65**:1137–1142



16. Merkler D., et al. (2006) **Myelin oligodendrocyte glycoprotein-induced experimental autoimmune encephalomyelitis in the common marmoset reflects the immunopathology of pabern II multiple sclerosis lesions** *Mult Scler* **12**:369–374
17. Brink B. P., et al. (2005) **The pathology of multiple sclerosis is location-dependent: no significant complement activation is detected in purely cortical lesions** *J Neuropathol Exp Neurol* **64**:147–155
18. Magliozzi R., Columba-Cabezas S., Serafini B., Aloisi F. (2004) **Intracerebral expression of CXCL13 and BAFF is accompanied by formation of lymphoid follicle-like structures in the meninges of mice with relapsing experimental autoimmune encephalomyelitis** *J Neuroimmunol* **148**:11–23
19. Bhargava P., et al. (2021) **Imaging meningeal inflammation in CNS autoimmunity identifies a therapeutic role for BTK inhibition** *Brain* **144**:1396–1408
20. Kueckelhaus J., et al. (2020) **Inferring Spatially Transient Gene Expression PaIern from Spatial Transcriptomic Studies** *bioRxiv* <https://doi.org/10.1101/2020.10.20.346544>
21. Hafemeister C., Satija R (2019) **Normalization and variance stabilization of single-cell RNAseq data using regularized negative binomial regression** *Genome Biology* **20**
22. Gene Ontology Consortium (2021) **The Gene Ontology resource: enriching a GOld mine** *Nucleic Acids Res* **49**:D325–D334
23. Ashburner M., et al. (2000) **Gene ontology: tool for the unification of biology. The Gene Ontology Consortium** *Nat Genet* **25**:25–29
24. Wu T., et al. (2021) **clusterProfiler 4.0: A universal enrichment tool for interpreting omics data** *The Innovation* **2**
25. Schubert M., et al. (2018) **Perturbation-response genes reveal signaling footprints in cancer gene expression** *Nat Commun* **9**
26. Yu G. (2023) **enrichplot: Visualization of Functional Enrichment Result**
27. Benjamini Y., Hochberg Y (1995) **Controlling the False Discovery Rate: A Practical and Powerful Approach to Multiple Testing** *Journal of the Royal Statistical Society: Series B (Methodological)* **57**:289–300
28. Bedussi B., et al. (2017) **Paravascular channels, cisterns, and the subarachnoid space in the rat brain: A single compartment with preferential pathways** *J Cereb Blood Flow Metab* **37**:1374–1385
29. Bhargava P., Hartung H.-P., Calabresi P. A (2022) **Contribution of B cells to cortical damage in multiple sclerosis** *Brain* **145**:3363–3373
30. Lisak R. P., et al. (2017) **B cells from patients with multiple sclerosis induce cell death via apoptosis in neurons in vitro** *Journal of Neuroimmunology* **309**:88–99
31. Benjamins J. A., et al. (2019) **Exosome-enriched fractions from MS B cells induce oligodendrocyte death** *Neurology - Neuroimmunology Neuroinflammation* **6**

32. Arellano G., Obum P. A., Reyes L. I., Burgos P. I., Naves R (2015) **Stage-Specific Role of Interferon-Gamma in Experimental Autoimmune Encephalomyelitis and Multiple Sclerosis** *Front. Immunol* **6**
33. Kirby L., et al. (2019) **Oligodendrocyte precursor cells present antigen and are cytotoxic targets in inflammatory demyelination** *Nature Communications* **10**
34. Schirmer L., et al. (2019) **Neuronal vulnerability and multilineage diversity in multiple sclerosis** *Nature* **573**:75–82
35. Falcão A. M., et al. (2019) **Disease-specific oligodendrocyte lineage cells arise in multiple sclerosis** *Nat Med* **24**:1837–1844
36. Jäkel S., et al. (2019) **Altered human oligodendrocyte heterogeneity in multiple sclerosis** *Nature* **566**:543–547
37. Langseth C. M., et al. (2023) **Single Cell-Resolution in Situ Sequencing Elucidates Spatial Dynamics of Multiple Sclerosis Lesion and Disease Evolution** *bioRxiv* <https://doi.org/10.1101/2023.06.29.547074>
38. Kukanja P., et al. (2024) **Cellular architecture of evolving neuroinflammatory lesions and multiple sclerosis pathology** *Cell* <https://doi.org/10.1016/j.cell.2024.02.030>
39. Lerma-Martin C., et al. (2022) **Spatial cell type mapping of multiple sclerosis lesions** *bioRxiv* <https://doi.org/10.1101/2022.11.03.514906>
40. Azevedo C. J., et al. (2018) **Thalamic Atrophy in Multiple Sclerosis: A Magnetic Resonance Imaging Marker of Neurodegeneration throughout Disease** *Ann Neurol* **83**:223–234
41. Magliozzi R., et al. (2022) **“Ependymal-in” Gradient of Thalamic Damage in Progressive Multiple Sclerosis** *Annals of Neurology* **92**:670–685
42. Gupta K., et al. (2023) **BAFF blockade in experimental autoimmune encephalomyelitis reduces inflammation in the meninges and synaptic and neuronal loss in adjacent brain regions** *J Neuroinflammation* **20**
43. Silva B. A., Miglieba E., Ferrari C. C (2021) **Neuroinflammation in cortical and meningeal pathology in multiple sclerosis: understanding from animal models** *Neuroimmunology and Neuroinflammation* **8**:174–184
44. James Bates R. E., et al. (2022) **Lymphotoxin-alpha expression in the meninges causes lymphoid tissue formation and neurodegeneration** *Brain* **145**:4287–4307
45. James R. E., et al. (2020) **Persistent elevation of intrathecal pro-inflammatory cytokines leads to multiple sclerosis-like cortical demyelination and neurodegeneration** *Acta Neuropathol Commun* **8**
46. Newton Y., et al. (2020) **Large scale, robust, and accurate whole transcriptome profiling from clinical formalin-fixed paraffin-embedded samples** *Sci Rep* **10**
47. Gracia Villacampa E., et al. (2021) **Genome-wide spatial expression profiling in formalin-fixed tissues** *Cell Genomics* **1**

## Editors

Reviewing Editor

**Irene Salinas**

University of New Mexico, Albuquerque, United States of America

Senior Editor

**Satyajit Rath**

Indian Institute of Science Education and Research (IISER), Pune, India

### Reviewer 1 (Public Review):

Multiple sclerosis (MS) is a debilitating autoimmune disease that causes loss of myelin in neurons of the central nervous system. MS is characterized by the presence of inflammatory immune cells in several brain regions as well as the brain barriers (meninges). This study aims to understand the local immune hallmarks in regions of the brain parenchyma that are adjacent to the leptomeninges in a mouse model of MS. The leptomeninges are known to be a foci of inflammation in MS and perhaps "bleed" inflammatory cells and molecules to adjacent brain parenchyma regions. To do so, they use novel technology called spatial transcriptomics so that the spatial relationships between the two regions remain intact. The study identifies canonical inflammatory genes and gene sets such as complement and B cells enriched in the parenchyma in close proximity to the leptomeninges in the mouse model of MS but not control. The manuscript is very well written and easy to follow. The results will become a useful resource to others working in the field and can be followed by time series experiments where the same technology can be applied to the different stages of the disease.

Comments on revised version:

I agree that the authors successfully addressed most of my comments/critiques. However, the fact that the control mice were not injected with CFA is somewhat concerning, because it will be hard to interpret the cause of the transcriptomic readouts described in this study. Some of the described effects might be due to CFA (which was used in the EAE but not the "naive" group), and not necessarily to the relapsing-remitting EAE immune features recapitulated in this mouse model. Moreover, this caveat associated with the "naive" control group is not being clearly stated throughout the manuscript and might go unnoticed to readers.

The authors should clearly state, in the methods section (in the section "Induction of SJL EAE"), that the naive control group was not injected with CFA.

Additionally, this potential confounder, of not using a control group injected with the same CFA regimen of the EAE group, should be mentioned in paragraph two of the discussion alongside the other limitations of the study already highlighted by the authors (or in another section of the discussion).

<https://doi.org/10.7554/eLife.88414.2.sa1>

### Reviewer 2 (Public Review):

Accumulating data suggests that the presence of immune cell infiltrates in the meninges of the multiple sclerosis brain contributes to the tissue damage in the underlying cortical grey matter by the release of inflammatory and cytotoxic factors that diffuse into the brain parenchyma. However, little is known about the identity and direct and indirect effects of these mediators at a molecular level. This study addresses the vital link between an adaptive immune response in the CSF space and the molecular mechanisms of tissue damage that

drive clinical progression. In this short report the authors use a spatial transcriptomics approach using Visium Gene Expression technology from 10x Genomics, to identify gene expression signatures in the meninges and the underlying brain parenchyma, and their interrelationship, in the PLP-induced EAE model of MS in the SJL mouse. MRI imaging using a high field strength (11.7T) scanner was used to identify areas of meningeal infiltration for further study. They report, as might be expected, the upregulation of genes associated with the complement cascade, immune cell infiltration, antigen presentation, and astrocyte activation. Pathway analysis revealed the presence of TNF, JAK-STAT and NFkB signaling, amongst others, close to sites of meningeal inflammation in the EAE animals, although the spatial resolution is insufficient to indicate whether this is in the meninges, grey matter, or both.

UMAP clustering illuminated a major distinct cluster of upregulated genes in the meninges and smaller clusters associated with the grey matter parenchyma underlying the infiltrates. The meningeal cluster contained genes associated with immune cell functions and interactions, cytokine production, and action. The parenchymal clusters included genes and pathways related to glial activation, but also adaptive/B-cell mediated immunity and antigen presentation. This again suggests a technical inability to resolve fully between the compartments as immune cells do not penetrate the pial surface in this model or in MS. Finally, a trajectory analysis based on distance from the meningeal gene cluster successfully demonstrated descending and ascending gradients of gene expression, in particular a decline in pathway enrichment for immune processes with distance from the meninges.

Comments on revised version:

The authors have addressed all of my comments regarding the lack of spatial resolution between the grey matter and the overlying meninges and also concerning the difficulties in extrapolating from this mouse model to MS itself.

I am however very concerned about the lack of the correct control group. Immunization of rodents with complete freunds adjuvant (albeit with pertussis toxin) gives rise to widespread microglial activation, some immune cell infiltration and also structural changes to axons, particularly at nodes of Ranvier (<https://doi.org/10.1097/NEN.0b013e3181f3a5b1>). This will inevitably make it difficult to interpret the transcriptomics results, depending on whether these changes are reversible or not and the time frame of the reversal. In the C57Bl6 EAE models adjuvant induced microglial activation becomes chronic, whereas the axonal changes do reverse by 10 weeks. Whether this is the same in SJL EAE model using CFA alone is not clear.

<https://doi.org/10.7554/eLife.88414.2.sa0>

#### Author response:

The following is the authors' response to the original reviews.

##### **Reviewer #1 (Recommendations For The Authors):**

*This study is very well framed and the writing is very clear. The manuscript is well organized and easy to follow and overall the previous state of the art of the field is taken into account. I only have a couple of minor comments*

*(1) There is a preprint that uses single nuclei RNA-Seq and ST on human MS subcortical white matter lesions doi: <https://doi.org/10.1101/2022.11.03.514906>. This work needs to be included in the discussion of the results.*



(1.1) We appreciate the reviewer bringing up this important preprint, and we have referenced it in the Discussion section of our updated manuscript.

*(2) The discussion should include the overall limitations of the study and how much it can be translated to human MS. Specifically, the current work uses EAE and therefore different disease stages are not captured in this study. This point is also raised by other reviewers.*

(1.2) We thank the reviewer for raising this important point, and we have included additional discussion about the limitations of EAE and its disease relevance to MS.

**Reviewer #2 (Recommendations For The Authors):**

*The authors state that this EAE model is better for studying cortical gradients because previous models "such as directly injecting inflammatory cytokines into the meninges/cortex" cause a traumatic injury. It needs to be discussed that these models have now been superseded by more refined models involving long-term overexpression of pro-inflammatory cytokines in the sub-arachnoid space, thereby avoiding traumatic injury. The current results should be discussed in light of these newer models (James et al, 2020; 2022), which are more similar to MS cortical pathology and do exhibit lymphoid-like structures.*

(2.1) We thank the reviewer for pointing out these relevant studies, and we agree they describe non-traumatic and more MS-relevant models of leptomeningeal inflammation. We have included discussion of these works in the updated manuscript.

- The study will be substantially improved if some of the ST data is validated at least partially with some RNAscope or other in situ hybridization using a subset of probes that capture the take-home message of the paper.*

(2.2) We agree with the reviewer that validation of transcriptomics results is important to support our conclusions. In the updated manuscript Figure 5 and Supplemental Figure 6 we have added RNAscope results for relevant genes. In agreement with the trends noted in the manuscript, expression of genes related to antigen processing and presentation such as *B2m* decreases gradually with distance from LMI. We also have included a reference to a newly published manuscript from our group (Gupta et al., 2023, J. Neuroinflammation) that characterizes meningeal inflammation and sub-pial changes in the SJL EAE model. In that manuscript, IHC is used to show accumulation of B cells and T cells in the leptomeningeal space, increased microglial and astrocyte reactivity adjacent to leptomeningeal inflammation, and reduction of neuronal markers adjacent to leptomeningeal inflammation.

- The lack of change in signaling pathways involved in B-cell/T-cell interaction and cytokine/chemokine signaling, which would be expected in areas of immune cell aggregation in the meninges, needs discussion.*

(2.3) While we detected significant upregulation in antigen presentation, complement activation, and humoral immune signaling, areas of meningeal inflammation identified as cluster 11 showed upregulation of numerous other GO gene sets associated with immune cell interaction and cytokine signaling, as described in supplementary table 3. These include T-cell receptor binding, CCR chemokine receptor binding, interleukin 8 production, response to interleukin 1, positive regulation of interleukin-6 production, tumor necrosis factor production, leukocyte cell-cell adhesion. Overall, we believe that the collection of enriched gene sets is consistent with peripheral myeloid and lymphoid infiltration and cytokine

production, with the most prominent cytokine / pathways being interferon  $\gamma$ /antigen processing and presentation, complement, and humoral inflammation.

- *Fig 4 subclusters includes T-cell activation, pos regulation of neuronal death, cellular response to IFN $\gamma$ , neg regulation of neuronal projections, Ig mediated immune response, cell killing, pos regulation of programmed cell death, pos regulation of apoptotic process, but none of these are discussed despite their obvious importance.*

(2.4) We agree with the reviewer that these upregulated genesets warrant additional discussion and have added additional reference to these genesets in the results section. Also, the genesets ‘positive regulation of programmed cell death’, ‘positive regulation of apoptotic process’, and ‘positive regulation of cell death’ were erroneously included in Figure 4F in the initial manuscript, as they are actually downregulated in cluster 1\_4. This has been clarified in the text.

- *Subcluster 11 appears spatially to represent the meninges, but what pathways are expressed there? 330 genes/pathways altered independent of other clusters - immune cell regulation?*

(2.5) We refer the reviewer to Supplementary Table 3, which contains a complete list of GO genesets enriched within cluster 11 spots.

- *The surprising lack of immunoglobulin genes upregulated in the meninges of the mice, considering these are the genes most upregulated in the MS meninges. Should be pointed out and discussed.*

(2.6) We appreciate the reviewer bringing up immunoglobulin genes, which previous publications have shown are elevated in MS meninges and cortical grey matter lesions. Consistent with this, several immunoglobulin genes are elevated in cluster 11, including genes encoding IgG2b, IgA, and IgM. While these results were available within the original submission in Supplementary Table 2, we have included the graph in the updated Supplementary Figure 3.

- *Meningeal signature may be poorly represented given the individual slices shown in suppl 3A, which suggests that only 3 of the EAE slices had significant meningeal infiltrates, indicated by cluster 11 genes.*

(2.7) There was heterogeneity in the location and extent of meningeal infiltrate / cluster 11 in the EAE slices, as the reviewer points out. 2 slices had severe inflammation, 2 had moderate inflammation, and 2 had relatively mild inflammation, but all EAE slices were enriched in inflammation relative to naïve as demonstrated not only through clustering, but also through enriched marker analysis between EAE and Naive and Progeny analysis.

- *The ST is not resolving the meningeal tissue and the immediate underlying grey matter, as demonstrated by a high signal for both CXCL13 and GFAP in cluster 11.*

(2.8) We agree that the spatial transcriptomics strategy applied here is inadequate to precisely delineate between meningeal inflammation and the underlying brain parenchyma, and that the elevation of markers such as GFAP in cluster 11 indicates some ‘contamination’ of parenchymal cells into cluster 11. We have clarified this in the text and discussed the limitation of the spatial transcriptomics method used.

- *More information is required concerning how many animals were used in this study, to meet the requirements for complying with the 3Rs.*

(2.9) A total of 4 mice were used per group. In the naïve group one mouse contributed two slices, for a total of 5 naïve slices. In the EAE group two mice contributed two slices, for a total of 6 EAE slices. We have clarified this in the methods section of the updated manuscript.

**Reviewer #3 (Recommendations For The Authors):**

*The authors should provide a more thorough description of the methodology, and there are a few minor concerns about experimental details, data presentation, and description that need to be addressed. In the next few lines, I will highlight a few important aspects that need to be addressed, propose some changes to the main manuscript, and suggest some additional experiments that, if successful, could confirm/support/further strengthen the conclusions that are at this point purely based on transcriptomic data.*

*Major comments/suggestions:*

- *The main gene expression changes between the control and EAE groups obtained via spatial transcriptomics need to be validated with another technique, at least partially. I suggest performing RNAscope or immunofluorescence imaging using brain sections from a new and independent cohort of animals, where cell-specific markers can also be tested. This type of assessment would work as a validation method and could also inform about the cell-specific contribution to the observed transcriptomic changes.*

(3.1) Please refer to response 2.2

- *The representative qualitative spatial expression heatmaps for each gene in Fig. 1F should be accompanied by corresponding graphs with quantitative measurements. Similar to what is done regarding the data in Fig. 2B and D.*

(3.2) We agree with the reviewer that quantitative graphs were missing, and we have included them in the updated Supplementary Figure 1.

- *A supplementary table discriminating all the DEGs (132 up and 70 downregulated) between cluster 11 and the other clusters has to be provided. What is the contribution of recruited encephalitogenic adaptive immune cells to this cluster 11 gene signature?*

(3.3) These unfiltered results are provided in Supplementary Table 2, and to view the up and down regulated genes the reader can sort the table based on fold change and adjusted P value. We believe providing the complete table is more useful to the reader, since the fold change and

P value thresholds used to determine “significance” are arbitrary. Since the spatial transcriptomics method used in this work does not have single cell resolution, we cannot accurately estimate the contribution of encephalitogenic adaptive immune cells in cluster 11. However, given previously published work of lymphocyte infiltration into the subarachnoid space in SJL EAE (Gupta et al., 2023, J. Neuroinflammation) and the enrichment of *Cd3e* in cluster 11 (Log2FC 0.31, adjusted P-val 0.005) we assume some contribution of peripheral lymphocytes.

- *The authors mention that there is grey matter pathology in this relapse model, and this has been shown in a previous publication (Bhargava et al., 2021). However, the regions analyzed in the present study are different from the ones shown in the referenced paper. Is there an overexpression of genes involved in, or gene modules indicative of, neuronal stress and/or death that spatially overlap with clusters 1 and 2? If so, it would be important to provide information about those gene modules in the main figures. It would also be quite relevant to show the levels of cell stress/death proteins and of axonal stress/damage, by APP and/or nonphosphorylated SMI-32 staining, in the deep brain regions (like the thalamus), to corroborate the link between these phenomena and the gene signatures of subclusters 1\_3, 1\_4, and 2\_6.*

(3.4) We thank the review for this insightful comment. We have recently published a manuscript that histologically analyzes leptomeningeal inflammation in the SJL EAE model, specifically assessing the areas looked at in our submitted manuscript (Gupta et al., 2023, J. Neuroinflammation). In that manuscript, IHC is used to show accumulation of B cells and T cells in the leptomeningeal space, increased microglial and astrocyte reactivity adjacent to leptomeningeal inflammation, and reduction of neuronal markers adjacent to leptomeningeal inflammation. To further describe the gene modules in the inflammatory subclusters 1\_3/1\_4/2\_6, we have now provided heatmaps of the selected genesets and their constituent genes (Supplementary Figure 5).

- *It would be important to provide heatmaps discriminating the DEGs that make the gene modules that are significantly altered in subclusters 1\_3, 1\_4, and 2\_6. The gene ontology terms are sometimes ambiguous. For instance, it would be very informative to the reader (and to the field) to know which altered genes compose the "lysosome", "immune response", "response to stress", or "B cell mediated immunity" pathways that are altered in the EAE subcluster 1\_3 (Fig. 4E). The same applies to the gene modules altered in the other subclusters of interest. Authors should also consider generating a Venn diagram with the DEGs from subclusters 1\_3, 1\_4, and 2\_6, to complement the GO term Venn presented in Fig. 4H. Having these pieces of information readily available, either as main or supplementary figures, would be a great addition.*

(3.5) We agree with the reviewer on this point and have included these heatmaps in Supplementary Figure 5.

- *The role of IFN-gamma as well as B cells (and Igs) in myelination/remyelination is mentioned in the discussion. However, there is very little evidence that these cells or their cytokines/Igs are mediating the described transcriptomic signatures at the level of the brain parenchyma of EAE mice undergoing relapse. Do the "antigen processing and presentation, cell killing, interleukin 6 production, and interferon gamma response" go terms, which better fitted the trajectory analysis, in fact include genes expressed almost exclusively by T and/or B cells? Are there genes that are downstream of IFN type I or II signaling?*

(3.6) Pathways including antigen processing / presentation, humoral inflammation, complement, among others were enriched in areas of meningeal inflammation and adjacent areas of parenchyma. These signaling pathways are mediated by effector molecules, many of which are produced by lymphocytes, but that can act on cells within the CNS parenchyma. The heatmaps in Supplementary Figure 5 demonstrate the significant role of MHC and



complement genes, which could be expressed by leukocytes as well as glia, on many of the pathways.

- *Is the transcriptomic overlap between meningeal and brain parenchymal regions, or the appearance of signatures similar to the parenchymal subclusters 1\_3, 1\_4, and 2\_6, prevented if the mice are treated with the murine versions of natalizumab or rituximab prior relapse?*

(3.6) We appreciate the reviewers suggestion. Our future directions for this work includes testing the effects of disease modifying therapies on spatial and single-cell transcriptomic readouts of disease in SJL EAE.

- *Please clarify what control group was used in this study. Naïve mice are mentioned in the Results section, does this mean that control animals were not injected with CFA? Authors should also elaborate on the descriptive methodology employed for the analysis of the spatial*

transcriptomics data - especially regarding the trajectory analysis. As is, overall, the methodology description might not favor reproducibility.

(3.7) We appreciate the need for clarification here. Our control group in this study was naïve, not having received any CFA or pertussis toxin. While often used as the control in EAE studies focused on mechanisms of autoimmunity, CFA and pertussis toxin independently induce systemic inflammation. Since in this study we were interested in neuroinflammation broadly, we chose to use a naïve comparison group to maximize our ability to find genes enriched in neuroinflammation. We have elaborated our methods section, including methods related to trajectory analysis.

*Minor comments/suggestions:*

*In Fig. 1D the indication of the rostral to ventral axis needs to be inverted.*

Addressed.

*In Fig. 1E the authors should also include a representative H&E staining of the same region in a control animal.*

Addressed.

*There is inconsistency in the number of clusters obtained after UMAP unbiased clustering of the spatial transcriptomic data:*

- *Fig. 3A-E - twelve clusters are shown (cluster 0 to 11).*
- *In the Results section eleven clusters are mentioned - "we performed unbiased UMAP clustering on the spatial transcriptomic dataset and identified 11 distinct clusters".*

The text was incorrect, there were 12 distinct clusters. This has been corrected.

*Considering the mice strain used was SJL/J mice, the peptide used to induce EAE should be PLP139-151, as mentioned in the Methods section "Induction of SJL EAE". However, the legend of Fig. 1 mentions "post immunization with MOG 35-55". Please correct this.*

Corrected.

*In the Methods section it is mentioned "At 12 weeks post-immunization, animals were euthanized", however the Results section mentions that tissues were harvested at 11 weeks post-immunization - "Brain slices were collected from four naïve mice and four EAE mice 11 weeks postimmunization". Please correct this.*

The Methods were incorrect, this has now been fixed.

*Please clarify the number of animals used for spatial transcriptomic analysis:*

- *Legend of Fig. 1 mentions "Red arrows indicate MRI time points, black arrow indicates time of tissue harvesting (N = 6)." Whilst in the Results section it states "Brain slices were collected from four naïve mice and four EAE mice".*

The figure one legend has now been corrected (N = 4). Additionally, we have added clarification about the number of animals / slices used in the Methods section (see response 2.9).

*Please be consistent in the way of representing DEGs in the MA plots:*

- *Fig. 3F shows the upregulated genes (in red) on the right and the downregulated genes (in blue) on the left.*
- *Supplemental Fig. 2K shows the upregulated genes (in red) on the left and the downregulated genes (in blue) on the right.*
- *Supplemental Fig. 4 shows the upregulated genes on the right in blue, while the downregulated genes are in red.*

This has been fixed.

*The letters attributed to each subcluster in panels E-G of Fig. 4 are different from the respective figure legend.*

This has been fixed.

*Correct the legend of supplemental figure 2: o "(G-H) Representative spatial feature plots of read count (F) and UMI (G) demonstrate expected anatomic variability in transcript amount and diversity."*

This has been fixed.

*In Supplemental Fig. 4G there is probably an error with the XX axis, since the significantly up and down-regulated genes are not visible.*

This has been fixed.

<https://doi.org/10.7554/eLife.88414.2.sa3>